

Article

# Ultra-Sensitive Hydrogen Peroxide Sensor Based on Peroxiredoxin and Fluorescence Resonance Energy Transfer

Haijun Yu <sup>1</sup>, Haoxiang Li <sup>1</sup>, Yao Zhou <sup>1</sup>, Shengmin Zhou <sup>1,\*</sup> and Ping Wang <sup>2</sup>

<sup>1</sup> State Key Laboratory of Bioreactor Engineering, School of Biotechnology, East China University of Science and Technology, Shanghai 200237, China; yuhj1115@163.com (H.Y.); haoxiang\_li8@126.com (H.L.); zhouyao\_04@163.com (Y.Z.)

<sup>2</sup> Department of Bioproducts and Biosystems Engineering, University of Minnesota, St Paul, MN 55108, USA; ping@umn.edu

\* Correspondence: zhoushengmin@ecust.edu.cn; Tel./Fax: +86-021-64250533

Received: 12 April 2020; Accepted: 17 May 2020; Published: 19 May 2020



**Abstract:** In this paper, a fluorescence resonance energy transfer (FRET)-based sensor for ultra-sensitive detection of H<sub>2</sub>O<sub>2</sub> was developed by utilizing the unique enzymatic properties of peroxiredoxin (Prx) to H<sub>2</sub>O<sub>2</sub>. Cyan and yellow fluorescent protein (CFP and YFP) were fused to Prx and mutant thioredoxin (mTrx), respectively. In the presence of H<sub>2</sub>O<sub>2</sub>, Prx was oxidized into covalent homodimer through disulfide bonds, which were further reduced by mTrx to form a stable mixed disulfide bond intermediate between CFP-Prx and mTrx-YFP, inducing FRET. A linear quantification range of 10–320 nM was obtained according to the applied protein concentrations and the detection limit (LOD) was determined to be as low as 4 nM. By the assistance of glucose oxidase to transform glucose into H<sub>2</sub>O<sub>2</sub>, the CFP-Prx/mTrx-YFP system (CPmTY) was further exploited for the detection of glucose in real sample with good performance, suggesting this CPmTY protein sensor is highly practical.

**Keywords:** hydrogen peroxide; biosensors; peroxiredoxin; thioredoxin

## 1. Introduction

Hydrogen peroxide (H<sub>2</sub>O<sub>2</sub>) is a strong oxidant, which is widely used in bleaching agents [1,2] and disinfectant [3,4]. In vivo, it is a main component of reactive oxygen species (ROS), which has long been considered to be harmful to cells [5] and involved in the development of many diseases [6,7]. Nonetheless, it is also found to participate in many signaling pathways [8,9] and to help defend against microbe infection [10,11] and abiotic stress [12]. Moreover, it is a by-product of many enzymatic reactions [13,14], with glucose oxidase (GOX) as a typical example [15,16]. The unique and significant role of H<sub>2</sub>O<sub>2</sub> attracts great research interest in biosensor development because one can know the amount of specific enzyme substrate indirectly by measuring its quantity. Therefore, the detection of H<sub>2</sub>O<sub>2</sub> is of practical significance.

At this moment, quite a lot of methods exist to detect H<sub>2</sub>O<sub>2</sub>, and they can be classified into four categories: colorimetric [17], spectrophotometry [18], electrochemistry [19], and fluorescence [20]. Among these, fluorescence-based methods have shown advantages like high sensitivity, fast response, and ability to fulfill in situ measurement in organelles within the cell. Besides fluorescent small molecules [21] and various fluorescent nano materials [22], fluorescent protein (FP) is another frequently utilized constituent in H<sub>2</sub>O<sub>2</sub> biosensors.

Many proteins in cell recognize H<sub>2</sub>O<sub>2</sub> with high selectivity and sensitivity by the advantage of specific activity of biological enzymes towards their substrate. One can easily fuse these recognition

elements to FPs through regular genetic manipulations to construct H<sub>2</sub>O<sub>2</sub> probes. HyPer [23,24] and roGFP2-Orp1 [25,26] are two prototypes of this kind, which involve a single FP to measure the excitation ratio, and both are frequently exploited in H<sub>2</sub>O<sub>2</sub>-related biochemical research. Enyedi et al. [27] developed two fluorescence resonance energy transfer (FRET)-based H<sub>2</sub>O<sub>2</sub> probes, which were different from Hyper and roGFP2-Orp1, involving two FPs and measuring emission ratio other than excitation. Compared to single FP, FRET-based protein sensors are easier to construct, and it is unnecessary to optimize the insertion site of response element into FP, and their ratiometric readouts can eliminate background interference. To the best of our knowledge, these are the only two pioneers in this type, therefore we would like to explore more. Peroxiredoxin (Prx) is a ubiquitous antioxidant protein [28]. As a member of the Prx family, Prx2 reacts with H<sub>2</sub>O<sub>2</sub> to form two intermolecular disulfide bonds in a homodimer, which can be reduced by thioredoxin/thioredoxin reductase (Trx/TrxR) system [29]. Both Prx and Trx were fused to a single FP to construct two efficient genetic redox probes, roGFP2-Prx [30] and TrxRFP [31], respectively. It was reported that transient mixed disulfide bond existed between Prx and Trx during the PRx reduction process [32], as verified by the observation of stable intermediate of mixed disulfide dimer between Trx active-site cysteine mutant (mTrx) and Prx [33,34]. This stable intermediate inspired us to construct a Prx/mTrx and FRET-based H<sub>2</sub>O<sub>2</sub> probe. In fact, at the same time as conducting this study, we also employed this Prx/mTrx combination to develop a cpYFP-based H<sub>2</sub>O<sub>2</sub> sensor and have recently proved its feasibility [35].

In the present study, we chose cyan fluorescent protein (CFP) and yellow fluorescent protein (YFP) as the energy donor and acceptor, respectively, to construct two fusion proteins of CFP-Prx and mTrx-YFP. After the addition of H<sub>2</sub>O<sub>2</sub> to the mixture of these two fusion proteins (CPmTY), the FRET ratio increased immediately as a result of the CFP-Prx/mTrx-YFP heterodimer formation through a mixed disulfide bond, showing the feasibility of CPmTY as a H<sub>2</sub>O<sub>2</sub> probe. CPmTY exhibited high sensitivity and good selectivity towards H<sub>2</sub>O<sub>2</sub>. The maximum emission ratio increase is much greater than precedent ones [27] and thus much more sensitive. Further research also indicates good performance of CPmTY in glucose detection by the transformation of glucose into H<sub>2</sub>O<sub>2</sub> with GOX.

## 2. Materials and Methods

### 2.1. Reagents

GOX (from *Aspergillus niger*) and dithiothreitol (DTT) were purchased from Aladdin Industrial Corporation. Hydrogen peroxide (35 wt% solution in water, stabilized) was bought from Acros Organics. Glucose and other reagents supplied by Sinopharm Chemical Reagent co. Ltd. are of analytical grade and used without further purification. Tert-butyl hydroperoxide (t-BOOH), cystine, oxidized glutathione (GSSG), xanthine, xanthine oxidase and 3-morpholininosydnonimine (SIN-1) were all obtained from Sigma-Aldrich.

### 2.2. Protein Expression and Purification

Trx (NCBI ACCESSION: XM\_652682.1) and Prx (NCBI ACCESSION: XM\_676869.1) utilized in this study were both from *Aspergillus nidulans*. Cysteine to serine mutation (C39S) in Trx was incorporated by site-directed mutagenesis according to the instruction manual of QuikChange™ Site-Directed Mutagenesis Kit from Stratagene, and the PCR kit of Premix PrimeSTAR HS (Takara, Code No.: R040A) was used in the experiment. CFP (mTurquoise2) was cloned into pET-28a (+) plasmid and the intermediate plasmid P1 obtained. Then, Prx was cloned into P1 at the 3' end of CFP by restriction enzyme digestion and ligation with linker sequence between them and the final expression plasmid P2 (for chimeric protein CFP-Prx) was obtained. YFP (mNeonGreen) and mTrx (TrxC39S) were cloned into pET-28a (+) by similar method to get expression plasmid P4 (for chimeric protein mTRX-YFP). Expression plasmid (P2 or P4) was transformed in to competent *E. coli* BL21 (DE3) through heat shock at 42 °C for 90 s, and protein synthesis was induced with 0.1 mM isopropyl thiogalactoside (IPTG) at

30 °C. Protein purification was conducted by affinity chromatography with Ni-NTA agarose according to the QIAexpressionist™ handbook (QIAGEN, Cat No.: 30210).

### 2.3. SDS-PAGE

Protein was analyzed by nonreducing 12% SDS-PAGE and gels were made up in our own laboratory and stained by Coomassie brilliant blue. CFP-PRX and mTrx-YFP were reduced by adding DTT and passed through a desalting column pre-equilibrated with appropriate buffer. Subsequently, they were mixed together with equimolar ratio and treated with indicated concentration of H<sub>2</sub>O<sub>2</sub> at 30 °C for 5 min. At last excessive amount of N-Ethylmaleimide (NEM) was added after treatments to block remaining thiol groups prior to dilution in gel-loading buffer.

### 2.4. Fluorescence Measurement

Emission spectra were measured on an F-4600 fluorescence spectrophotometer (HITACHI, Tokyo, Japan) in a cuvette with excitation at 400 nm and emission from 460 to 560 nm. The FRET ratio (518 nm/476 nm) was then calculated from specific emission spectrum.

### 2.5. Selectivity Test

Oxidized glutathione, cysteine, tert-butyl hydroperoxide (t-BOOH), superoxide radicals and peroxynitrite anion (ONOO<sup>-</sup>) were exploited to test the selectivity of this detection method versus H<sub>2</sub>O<sub>2</sub>. Superoxide radicals were generated by xanthine–xanthine oxidase system and ONOO<sup>-</sup> by SIN-1.

### 2.6. Glucose Detection

An amount of 2 μL GOX (1 U/mL) and 10 μL glucose solution with various concentrations were mixed together. Then, 988 μL of CFP-Prx and mTrx-YFP mixture of equal molar ratio was added to GOX-glucose reaction system and the FRET ratio was measured. In this approach, the relation between glucose concentration and FRET ratio was established.

## 3. Results and Discussion

### 3.1. Construction of the Proposed H<sub>2</sub>O<sub>2</sub> Probe

We employed CFP and YFP to construct the proposed H<sub>2</sub>O<sub>2</sub> probe, as a FRET donor and acceptor, respectively. As shown in Figure 1, CFP was linked to Prx (to form Prx-CFP) and YFP to mutant Trx (to form mTrx-YFP). Two intermolecular disulfide bonds formed in Prx homodimer in the presence of H<sub>2</sub>O<sub>2</sub>, and then mTrx reacted with the homodimer to generate mixed disulfide dimers, bringing the tethered CFP and YFP close enough to generate FRET signals, which in reverse could indicate H<sub>2</sub>O<sub>2</sub> concentration in the medium. We named this new probe CPmTY, the abbreviation of the essential mixed disulfide dimer CFP-Prx/mTrx-YFP.

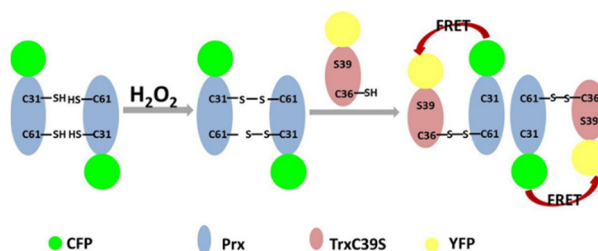


**Figure 1.** Schematic illustration of the working principle of proposed H<sub>2</sub>O<sub>2</sub> probe CFP-Prx/mTrx-YFP. CFP—cyan fluorescent protein, Prx—peroxiredoxin, mTrx—mutant thioredoxin, YFP—yellow fluorescent protein.

### 3.2. FRET Signals Respond to $H_2O_2$ Concentration as a Result of CFP-Prx/mTrx-YFP Conjugation through Disulfide Bond

CFP-Prx and mTrx-YFP were successfully expressed and purified in this work. The fluorescence properties of both FPs were not interfered in each chimeric protein. At the same time, CFP-Prx retained the ability to react with  $H_2O_2$  to form dimer as free Prx did. When mixing and adding  $H_2O_2$  into the mixture, CFP-Prx/mTrx-YFP heterodimer formed as verified by SDS-PAGE (Figure 2a). If one disulfide bond in Prx dimer remained, an mTRX and a PRX-CFP dimer formed a covalent heterotrimer. Otherwise, this heterotrimer further resolved by another mTrx-YFP and decomposed into two CFP-Prx/mTrx-YFP heterodimers. Therefore, there were five kinds of entities in the mixture with the presence of  $H_2O_2$  corresponding to the five bands in each lane of SDS-PAGE image from top to bottom: (1) CFP-Prx/CFP-Prx/mTrx-YFP heterotrimer, (2) CFP-Prx/CFP-Prx homodimer, (3) CFP-Prx/mTrx-YFP heterodimer, (4) monomer CFP-Prx, and (5) monomer mTrx-YFP, where (2) and (3) were very close to each other. Moreover, as the  $H_2O_2$  amount increased, the monomers decreased in concentration while the trimer and dimer increased. FRET happened between CFP-Prx and mTrx-YFP in hetero dimer and trimer, as revealed in the fluorescence spectra (Figure 2b). Each spectrum corresponds to one lane in the SDS-PAGE image and more hetero dimer and trimer lead to higher FRET signals (decrease of CFP fluorescence and increase of YFP's). In this way, the  $H_2O_2$  concentration can be reflected by the FRET signal intensity.

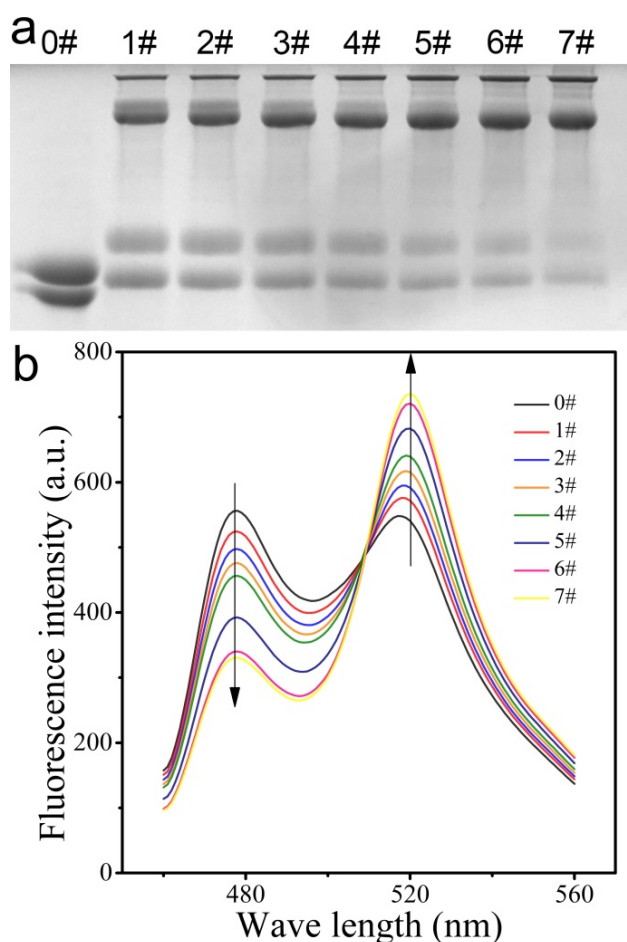


**Figure 2.** Demonstrations of  $H_2O_2$  induced homo/hetero dimerization between CFP-Prx and mTrx-YFP and corresponding fluorescence resonance energy transfer (FRET) signal changes. (a) SDS-PAGE of CFP-Prx and mTrx-YFP mixtures after reacting with  $H_2O_2$ , in 0# sample no  $H_2O_2$  existed, from 1# to 7# sample  $H_2O_2$  concentration increased gradually. (b) Fluorescence spectra of the same sample as indicated in panel (a).

To further prove that intermediate disulfide bonds was the cause for the FRET signal, we add DTT, which can destroy the bond, after  $H_2O_2$  and FRET signal diminished gradually in six minutes (Figure 3a). The reaction between DTT and protein disulfide bond was rather slow compared with that between Prx and  $H_2O_2$ , which completed in seconds. Thus we can measure the FRET signal immediately after  $H_2O_2$  addition, which is a benefit of this detection method. We also constructed wild-type Trx fused with YFP (wtTrx-YFP), which cannot induce FRET with CFP-Prx in the presence of  $H_2O_2$  (Figure 3b), as the resolving cysteine in wtTrx destroys the intermediate disulfide bond.

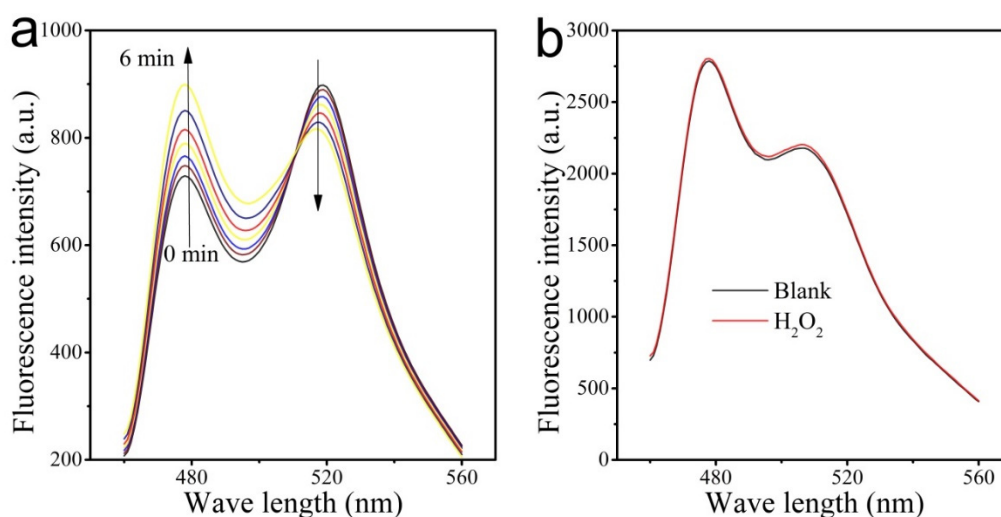


**Figure 3.** Confirmation of disulfide bonds formation as the mechanism of  $H_2O_2$  induced FRET in CFP-Prx/mTrx-YFP system (CPmTY). (a) Fluorescence spectrum variation in 6 min when excess amount of DTT was added after CPmTY reaction with and  $H_2O_2$ . (b) Fluorescence spectra of CFP-Prx/wtTrx-YFP (wild-type Trx that retained the resolving cysteine residue, C39) mixture in the absence (black line) and presence (red line) of abundant  $H_2O_2$ .

### 3.3. Ability of CPmTY to Detect $H_2O_2$ with Low Limit and Wide Range by Optimal Protein Concentration

First, we conducted the detection experiment in 20 mM Tris-HCl (pH 8.0) with 150 mM NaCl, the same buffer as used for protein purification. In this condition, the FRET ratio was very small, even after adding an excess amount of  $H_2O_2$  (much like Figure 3b). We then removed NaCl from the buffer and found the FRET ratio increased significantly in response to  $H_2O_2$  (much like Figure 2b). Salt ions may bind on protein interfaces to destroy hydrophobic interactions between protein dimer and prevent proteins from getting close to each other by electrostatic repulsion. Thus, NaCl may decrease the FRET ratio by impeding CFP-Prx dimerization and separating CFP and YFP in the CFP-Prx/mTrx-YFP conjugate. Moreover, YFP used in this study is pH sensitive, and shows stronger fluorescence intensity in pH 6–8. Therefore, we finally chose to examine the detection performance of CPmTY in 1 mM phosphate buffer (pH 7.0). Based on the working principle, the detection range of this method depends on the concentration of the two chimeric proteins. Here, we set the molar ratio as 1:1. With 200 nM CFP-Prx and 200 nM mTrx-YFP, the FRET ratio of CPmTY increased linearly in the range from 0 to 80 nM of  $H_2O_2$ . At a concentration four times of the former (i.e., 800 nM CFP-Prx and 800 nM mTrx-YFP) the linear range expanded to 120–320 nM. Based on these results, it could be concluded that  $H_2O_2$  detection range by CPmTY varies with CFP-Prx and mTrx-YFP protein concentrations. However, the protein concentrations should neither be too high nor too low. As the concentration increased, spontaneous FRET occurred between separate CFP-Prx and mTRX-YFP, diminishing detection sensitivity (i.e., the difference between largest and smallest FRET ratio). As shown in Figure 4, the slope of the left fitting curve (i.e., 0.01) is greater than four times of the right (i.e., 0.0015). If the protein concentrations continue to increase, slope value of the fitting curve would tend to be zero, meaning that spontaneous FRET between separate CFP-Prx and mTrx-YFP equals

to that within the CFP-Prx/mTrx-YFP conjugate. On the other hand, too low protein concentrations also damage detection performance, as the fluorescence intensity is similar to the background interference, and at the same time both reaction possibilities between reduced CFP-Prx and  $H_2O_2$  and between oxidized CFP-Prx dimer and mTrx-YFP decrease drastically.

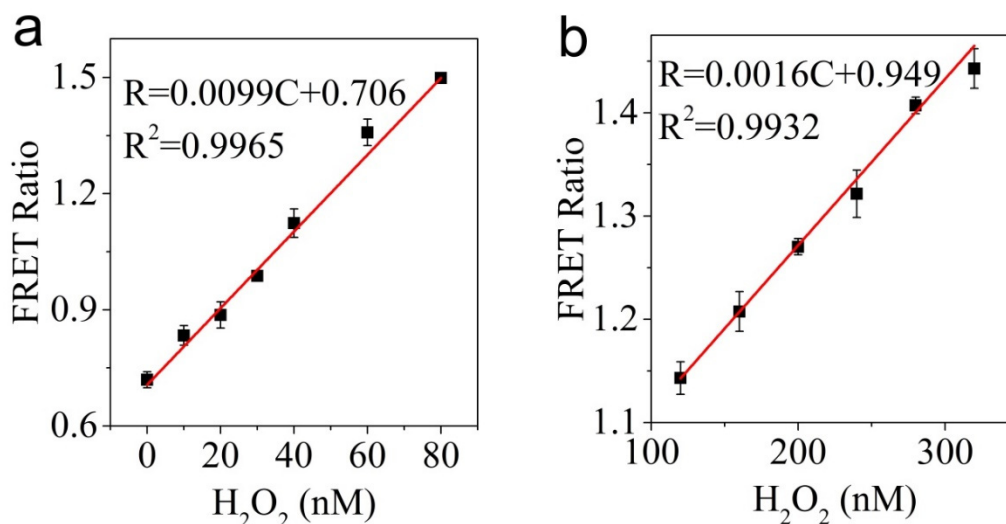


**Figure 4.** Titration curve of FRET in CPmTY over a serial of  $H_2O_2$  concentrations. (a) 200 nM CFP-Prx and 200 nM mTrx-YFP with 0, 10, 20, 30, 40, 60, 80 nM  $H_2O_2$ . (b) 800 nM CFP-Prx and 800 nM mTrx-YFP with 120, 160, 200, 240, 280, 320 nM  $H_2O_2$ .

The optimal detection limit of CPmTY was determined to be 4 nM (calculated as  $3S_B/m$ ,  $S_B$  is the standard deviation of 20 blank responses and  $m$  the slope of calibration curve), which was much lower than most of the present  $H_2O_2$  detection methods (as shown in Table 1). In the general detection test, we preferred to set the protein concentrations to a relatively low level to increase detection sensitivity. Hence, when applying a low detection range, the dilution of samples with high  $H_2O_2$  concentration can eliminate the interference of other compositions such as salts in the sample.

**Table 1.** Comparison of the performance of various  $H_2O_2$  sensors.

Method	Detection Limit	Linear Range	Reference
Enzymatic colorimetric detection	2.5 $\mu$ M	0.05–0.50 mM	[36]
Hybrid microflower enzymatic amperometric detection	50 $\mu$ M	100 $\mu$ M–100 mM	[19]
Small-molecule fluorescence detection	5.3 $\mu$ M		[37]
Small-molecule fluorescence detection	0.07 $\mu$ M	0.5–200 $\mu$ M	[18]
Small-molecule fluorescence detection	21 nM	3–500 $\mu$ M	[38]
Small-molecule fluorescence detection	25 nM	1–60 $\mu$ M	[39]
Small-molecule fluorescence detection	160 nM	5–20 $\mu$ M	[40]
Nanocomposite colorimetric detection	14 nM	0.01–30 $\mu$ M	[17]
Nanocomposite ratiometric fluorescence Detection	112 $\mu$ M	60–600 $\mu$ M	[22]
Nanocomposite nonenzymatic colorimetric detection	168 nM	0.5–10 $\mu$ M	[41]
Nanocomposite nonenzymatic fluorescence detection	3.87 nM	10 nM–10 mM	[42]
Nanocomposite nonenzymatic fluorescence detection	22 nM	30–300 nM	[42]
Nanocomposite nonenzymatic ratiometric fluorescence detection	11 nM	30–110 nM	[43]
Nanocomposite nonenzymatic amperometric detection	10 nM	0.025–5.0 $\mu$ M	[44]
Nanocomposite nonenzymatic amperometric detection	1.6 $\mu$ M	Up to 14 mM	[45]
Nanocomposite nonenzymatic amperometric detection	2.2 $\mu$ M	Up to 15 mM	[46]
Nanocomposite nonenzymatic amperometric detection	0.1 $\mu$ M	Up to 20 mM	[47]
Nanocomposite nonenzymatic amperometric detection	0.5 $\mu$ M	0.002–1.0 mM	[48]
Nanocomposite nonenzymatic amperometric detection	1 $\mu$ M	10 $\mu$ M–15 mM	[47]
Nanocomposite nonenzymatic amperometric detection	2 nM	12.64 nM–2104 $\mu$ M	[48]
Nanocomposite nonenzymatic photoelectrochemical detection	1.2 $\mu$ M	5–250 $\mu$ M	[48]
CFP-Prx/mTrx-YFP ratiometric fluorescence Detection	4 nM	10–320 nM	This study

### 3.4. Detection Selectivity

The detection of  $\text{H}_2\text{O}_2$  in cells or other biological samples is frequently interfered with other oxidants, so the performance of CPmTY was tested in the presence of potential interfering species. The results were shown in Figure 5. CPmTY did not react with most of them (superoxide anion, cysteine, oxidized glutathione, and peroxynitrite) and showed excellent selectivity to  $\text{H}_2\text{O}_2$ . The only exception is T-BOOTH, which is synthetic and does not exist in real samples. This selectivity may be ascribed to the high specificity of Prx to  $\text{H}_2\text{O}_2$ .

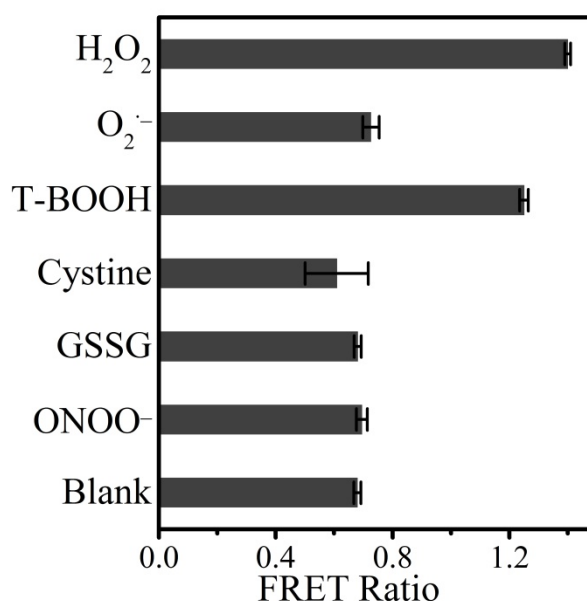


**Figure 5.** Interference of common oxidant on FRET signal of CPmTY. Concentration of oxidized glutathione (GSSG), cysteine, tert-butyl hydroperoxide (t-BOOH): 1  $\mu\text{M}$ ,  $\text{H}_2\text{O}_2$ : 100 nM, superoxide radicals ( $\text{O}_2^-$ ) and peroxynitrite anion ( $\text{ONOO}^-$ ) were produced in situ by specific enzymatic reactions as described in experimental section.

### 3.5. Detection of Glucose

Detection of glucose involves glucose oxidation by glucose oxidase to generate  $\text{H}_2\text{O}_2$  and the ensuing  $\text{H}_2\text{O}_2$  measurement. First, the quantitative relationship between glucose concentration and the FRET ratio was calibrated. The glucose solution was diluted to a serial of concentrations (0, 2, 4, 6, 8, 10, 12  $\mu\text{M}$ ), and reacted with GOX. Subsequently, CFP-Prx and mTrx-YFP mixture, both 150 nM, was added to the glucose oxidation system and fluorescence spectra were measured. The glucose oxidation was conducted in a small volume in order to obtain relatively higher enzyme and substrate concentration for fast and complete reaction. Figure 6 showed the corresponding fluorescence spectrum from each measurement, labeled by the glucose concentration. The FRET ratio (518 nm/476 nm) was calculated and plotted versus glucose concentration as a calibration curve (inset in Figure 6). Finally, the calibration equation of  $R = 0.0039C + 0.822$  ( $R^2 = 0.9809$ ) was obtained for the glucose analysis. Herein, R is the FRET ratio (518 nm/476 nm),  $R^2$  is correlation coefficient and C is the concentration of glucose (nM).

To verify the applicability of CPmTY for glucose detection, Dulbecco's modified eagle medium (DMEM, Corning Cat. No. 10-013) was tested with labeled glucose concentration of 4500 mg/L, that is, 25 mM. The result was 24.58 mM, indicating a recovery of  $98.32 \pm 0.47\%$  and confirming the applicability of CPmTY.

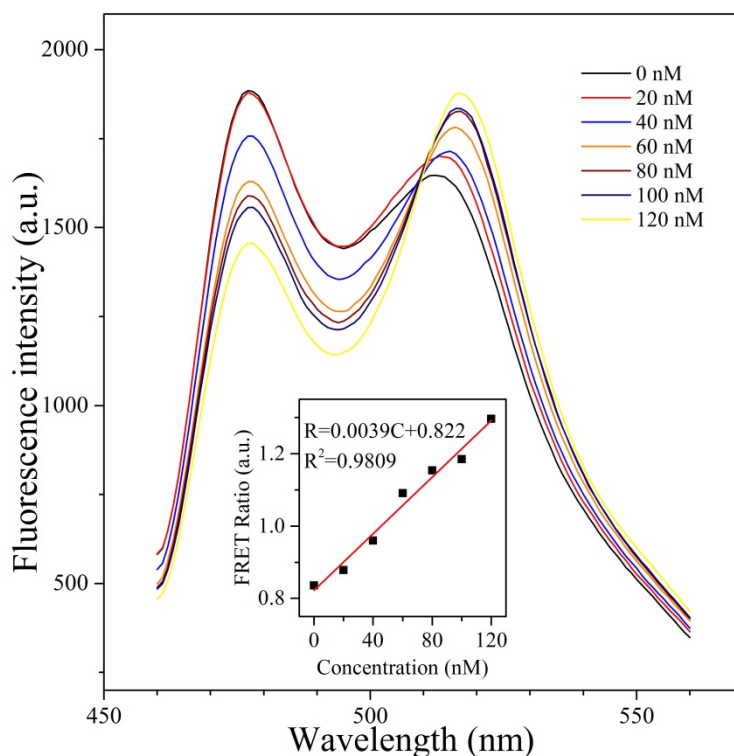


**Figure 6.** Detection of glucose with CPMTY. A serial of glucose solution reacted with glucose oxidase (GOX) and then the reaction products were added to 300 nM CFP-Prx and 300 nM mTrx-YFP mixtures, glucose concentrations indicated were the final ones in the detection mixtures.

#### 4. Conclusions

In this work, we developed a mild, sensitive, and fast detection method for  $H_2O_2$  by the distinctive reaction among  $H_2O_2$ , Prx, and mTrx, which can bring tethered CFP and YFP together to induce FRET. The detection limit was determined to be as low as 4 nM. This sensitive method shows satisfactory selectivity toward  $H_2O_2$  over other interfering oxidants. Moreover, this method can be applied to detect glucose content in DMEM with the aid of GOX and the result is very close to the labeled data. As there are numerous  $H_2O_2$  reacting proteins, such as Prx and  $H_2O_2$  transforming reactions, like GOX in nature, this study provides a novel idea to develop biosensors for  $H_2O_2$  and substances that can be transformed to  $H_2O_2$  by suitable enzymes.

**Author Contributions:** Conceptualization, H.Y.; Funding acquisition, S.Z. and P.W.; Investigation, H.Y. and H.L.; Methodology, H.Y. and Y.Z.; Supervision, P.W.; Writing—original draft, H.Y.; Writing—review & editing, S.Z. All authors have read and agreed to the published version of the manuscript.

**Funding:** This research was funded by National Science Foundation of China (21672065 and 21636003), the Fundamental Research Funds for the Central Universities (22221818014), the 111 Project (B18022), the Project Funded by the International S&T Innovation Cooperation Key Project (2017YFE0129600), and National Major Scientific and Technological Special Project for “Significant New Drugs Development” (2019ZX09739-001).

**Conflicts of Interest:** The authors declare no conflict of interest.

#### References

1. Tang, P.; Ji, B.; Sun, G. Whiteness Improvement of Citric Acid Crosslinked Cotton Fabrics:  $H_2O_2$  Bleaching under Alkaline Condition. *Carbohydr. Polym.* **2016**, *147*, 139–145. [[CrossRef](#)] [[PubMed](#)]
2. Bianchi, M.L.; Crisol, R.; Schuchardt, U. Bleaching of Commercial Pulp with  $H_2O_2$  Catalyzed by Heteropolyacids. *Bioresour. Technol.* **1999**, *68*, 17–21. [[CrossRef](#)]

3. Le Toquin, E.; Faure, S.; Orange, N.; Gas, F. New Biocide Foam Containing Hydrogen Peroxide for the Decontamination of Vertical Surface Contaminated With *Bacillus Thuringiensis* Spores. *Front. Microbiol.* **2018**, *9*, 1–11. [[CrossRef](#)] [[PubMed](#)]
4. Zhou, Y.; Li, C.; Hao, Y.; Ye, B.; Xu, M. Oriented Growth of Cross-Linked Metal-Organic Framework Film on Graphene Surface for Non-Enzymatic Electrochemical Sensor of Hydrogen Peroxide in Disinfectant. *Talanta* **2018**, *188*, 282–287. [[CrossRef](#)]
5. Pletjushkina, O.Y.; Fetisova, E.K.; Lyamzaev, K.G.; Ivanova, O.Y.; Domnina, L.V.; Vysokikh, M.Y.; Pustovidko, A.V.; Vasiliev, J.M.; Murphy, M.P.; Chernyak, B.V.; et al. Long-Distance Apoptotic Killing of Cells Is Mediated by Hydrogen Peroxide in a Mitochondrial ROS-Dependent Fashion. *Cell Death Differ.* **2005**, *12*, 1442–1444. [[CrossRef](#)]
6. Angelova, P.R.; Abramov, A.Y. Role of Mitochondrial ROS in the Brain: From Physiology to Neurodegeneration. *FEBS Lett.* **2018**, *592*, 692–702. [[CrossRef](#)]
7. Reczek, C.R.; Chandel, N.S. ROS Promotes Cancer Cell Survival through Calcium Signaling. *Cancer Cell* **2018**, *33*, 949–951. [[CrossRef](#)]
8. Mori, S.; Morihira, K.; Okuda, T.; Kasahara, Y.; Obika, S. Hydrogen Peroxide-Triggered Gene Silencing in Mammalian Cells through Boronated Antisense Oligonucleotides. *Chem. Sci.* **2018**, *9*, 1112–1118. [[CrossRef](#)]
9. Reczek, C.R.; Chandel, N.S. ROS-Dependent Signal Transduction. *Curr. Opin. Cell Biol.* **2015**, *33*, 8–13. [[CrossRef](#)]
10. Thiagarajah, J.R.; Chang, J.; Goettel, J.A.; Verkman, A.S.; Lencer, W.I. Aquaporin-3 Mediates Hydrogen Peroxide-Dependent Responses to Environmental Stress in Colonic Epithelia. *Proc. Natl. Acad. Sci. USA* **2017**, *114*, 568–573. [[CrossRef](#)]
11. Allaoui, A.; Botteaux, A.; Dumont, J.E.; Hoste, C.; De Deken, X. Dual Oxidases and Hydrogen Peroxide in a Complex Dialogue between Host Mucosae and Bacteria. *Trends Mol. Med.* **2009**, *15*, 571–579. [[CrossRef](#)] [[PubMed](#)]
12. Fedurayev, P.V.; Mironov, K.S.; Gabrielyan, D.A.; Bedbenov, V.S.; Zorina, A.A.; Shumskaya, M.; Los, D.A. Hydrogen Peroxide Participates in Perception and Transduction of Cold Stress Signal in *Synechocystis*. *Plant Cell Physiol.* **2018**, *59*, 1255–1264. [[CrossRef](#)] [[PubMed](#)]
13. Rocha-Martin, J.; Velasco-Lozano, S.; Guisán, J.M.; López-Gallego, F. Oxidation of Phenolic Compounds Catalyzed by Immobilized Multi-Enzyme Systems with Integrated Hydrogen Peroxide Production. *Green Chem.* **2014**, *16*, 303–311. [[CrossRef](#)]
14. Messner, K.R.; Imlay, J.A. Mechanism of Superoxide and Hydrogen Peroxide Formation by Fumarate Reductase, Succinate Dehydrogenase, and Aspartate Oxidase. *J. Biol. Chem.* **2002**, *277*, 42563–42571. [[CrossRef](#)]
15. Ferri, S.; Kojima, K.; Sode, K. Review of Glucose Oxidases and Glucose Dehydrogenases: A Bird's Eye View of Glucose Sensing Enzymes. *J. Diabetes Sci. Technol.* **2011**, *5*, 1068–1076. [[CrossRef](#)]
16. Tzanov, T.; Costa, S.A.; Gübitz, G.M.; Cavaco-Paulo, A. Hydrogen Peroxide Generation with Immobilized Glucose Oxidase for Textile Bleaching. *J. Biotechnol.* **2002**, *93*, 87–94. [[CrossRef](#)]
17. Teodoro, K.B.R.; Migliorini, F.L.; Christinelli, W.A.; Correa, D.S. Detection of Hydrogen Peroxide (H<sub>2</sub>O<sub>2</sub>) Using a Colorimetric Sensor Based on Cellulose Nanowhiskers and Silver Nanoparticles. *Carbohydr. Polym.* **2019**, *212*, 235–241. [[CrossRef](#)]
18. Zhou, Z.; Li, Y.; Su, W.; Gu, B.; Xu, H.; Wu, C.; Yin, P.; Li, H.; Zhang, Y. A Dual-Signal Colorimetric and near-Infrared Fluorescence Probe for the Detection of Exogenous and Endogenous Hydrogen Peroxide in Living Cells. *Sens. Actuators B Chem.* **2019**, *280*, 120–128. [[CrossRef](#)]
19. Zhang, M.; Chen, M.; Liu, Y.; Wang, Y.; Tang, J. Catalase-Inorganic Hybrid Microflowers Modified Glassy Carbon Electrode for Amperometric Detection of Hydrogen Peroxide. *Mater. Lett.* **2019**, *243*, 9–12. [[CrossRef](#)]
20. Liu, J.; Liang, J.; Wu, C.; Zhao, Y. A Doubly-Quenched Fluorescent Probe for Low-Background Detection of Mitochondrial H<sub>2</sub>O<sub>2</sub>. *Anal. Chem.* **2019**, *91*, 6902–6909. [[CrossRef](#)]
21. Zheng, D.J.; Yang, Y.S.; Zhu, H.L. Recent Progress in the Development of Small-Molecule Fluorescent Probes for the Detection of Hydrogen Peroxide. *TrAC Trends Anal. Chem.* **2019**, *118*, 625–651. [[CrossRef](#)]
22. Wang, H.; Li, Y.; Yang, M.; Wang, P.; Gu, Y. FRET-Based Upconversion Nanoprobe Sensitized by Nd<sup>3+</sup> for the Ratiometric Detection of Hydrogen Peroxide in Vivo. *ACS Appl. Mater. Interfaces* **2019**, *11*, 7441–7449. [[CrossRef](#)] [[PubMed](#)]

23. Belousov, V.V.; Fradkov, A.F.; Lukyanov, K.A.; Staroverov, D.B.; Shakhbazov, K.S.; Terskikh, A.V.; Lukyanov, S. Genetically Encoded Fluorescent Indicator for Intracellular Hydrogen Peroxide. *Nat. Methods* **2006**, *3*, 281–286. [[CrossRef](#)] [[PubMed](#)]
24. Bilan, D.S.; Pase, L.; Joosen, L.; Gorokhovatsky, A.Y.; Ermakova, Y.G.; Gadella, T.W.J.; Grabher, C.; Schultz, C.; Lukyanov, S.; Belousov, V.V. HyPer-3: A Genetically Encoded H<sub>2</sub>O<sub>2</sub> Probe with Improved Performance for Ratiometric and Fluorescence Lifetime Imaging. *ACS Chem. Biol.* **2013**, *8*, 535–542. [[CrossRef](#)]
25. Ermakova, Y.G.; Bilan, D.S.; Matlashov, M.E.; Mishina, N.M.; Markvicheva, K.N.; Subach, O.M.; Subach, F.V.; Bogeski, I.; Hoth, M.; Enikolopov, G.; et al. Red Fluorescent Genetically Encoded Indicator for Intracellular Hydrogen Peroxide. *Nat. Commun.* **2014**, *5*, 1–9. [[CrossRef](#)]
26. Gutscher, M.; Sobotta, M.C.; Wabnitz, G.H.; Ballikaya, S.; Meyer, A.J.; Samstag, Y.; Dick, T.P. Proximity-Based Protein Thiol Oxidation by H<sub>2</sub>O<sub>2</sub>-Scavenging Peroxidases. *J. Biol. Chem.* **2009**, *284*, 31532–31540. [[CrossRef](#)]
27. Enyedi, B.; Zana, M.; Donkó, Á.; Geiszt, M. Spatial and Temporal Analysis of NADPH Oxidase-Generated Hydrogen Peroxide Signals by Novel Fluorescent Reporter Proteins. *Antioxid. Redox Signal.* **2013**, *19*, 523–534. [[CrossRef](#)]
28. Rhee, S.G.; Woo, H.A.; Kil, I.S.; Bae, S.H. Peroxiredoxin Functions as a Peroxidase and a Regulator and Sensor of Local Peroxides. *J. Biol. Chem.* **2012**, *287*, 4403–4410. [[CrossRef](#)]
29. Peskin, A.V.; Pace, P.E.; Behring, J.B.; Paton, L.N.; Soethoudt, M.; Bachschmid, M.M.; Winterbourn, C.C. Glutathionylation of the Active Site Cysteines of Peroxiredoxin 2 and Recycling by Glutaredoxin. *J. Biol. Chem.* **2016**, *291*, 3053–3062. [[CrossRef](#)]
30. Morgan, B.; Van Laer, K.; Owusu, T.N.E.; Ezeriņa, D.; Pastor-Flores, D.; Amponsah, P.S.; Tursch, A.; Dick, T.P. Real-Time Monitoring of Basal H<sub>2</sub>O<sub>2</sub> Levels with Peroxiredoxin-Based Probes. *Nat. Chem. Biol.* **2016**, *12*, 437–443. [[CrossRef](#)]
31. Fan, Y.; Makar, M.; Wang, M.X.; Ai, H.W. Monitoring Thioredoxin Redox with a Genetically Encoded Red Fluorescent Biosensor. *Nat. Chem. Biol.* **2017**, *13*, 1045–1052. [[CrossRef](#)] [[PubMed](#)]
32. Lian, F.M.; Yu, J.; Xiao-Xiao, M.; Yu, X.J.; Chen, Y.; Zhou, C.Z. Structural Snapshots of Yeast Alkyl Hydroperoxide Reductase Ahp1 Peroxiredoxin Reveal a Novel Two-Cysteine Mechanism of Electron Transfer to Eliminate Reactive Oxygen Species. *J. Biol. Chem.* **2012**, *287*, 17077–17087. [[CrossRef](#)]
33. Kouwen, T.R.H.M.; Andréll, J.; Schrijver, R.; Dubois, J.Y.F.; Maher, M.J.; Iwata, S.; Carpenter, E.P.; van Dijl, J.M.; Thioredoxin, A. Active-Site Mutants Form Mixed Disulfide Dimers That Resemble Enzyme-Substrate Reaction Intermediates. *J. Mol. Biol.* **2008**, *379*, 520–534. [[CrossRef](#)] [[PubMed](#)]
34. Hisabori, T.; Hara, S.; Fujii, T.; Yamazaki, D.; Hosoya-Matsuda, N.; Motohashi, K. Thioredoxin Affinity Chromatography: A Useful Method for Further Understanding the Thioredoxin Network. *J. Exp. Bot.* **2005**, *56*, 1463–1468. [[CrossRef](#)] [[PubMed](#)]
35. Yang, Y.; Zhou, Y.; Li, J.; Yu, H.; Takaya, N.; Wang, P.; Zhou, S. Novel Peroxiredoxin-Based Sensor for Sensitive Detection of Hydrogen Peroxide. *Biochem. Biophys. Res. Commun.* **2019**, *517*, 260–265. [[CrossRef](#)] [[PubMed](#)]
36. Chen, Y.; Zhong, Q.; Wang, Y.; Yuan, C.; Qin, X.; Xu, Y. Colorimetric Detection of Hydrogen Peroxide and Glucose by Exploiting the Peroxidase-like Activity of Papain. *RSC Adv.* **2019**, *9*, 16566–16570. [[CrossRef](#)]
37. He, Y.; Miao, L.; Yu, L.; Chen, Q.; Qiao, Y.; Zhang, J.F.; Zhou, Y. A Near-Infrared Fluorescent Probe for Detection of Exogenous and Endogenous Hydrogen Peroxide in Vivo. *Dye. Pigment.* **2019**, *168*, 160–165. [[CrossRef](#)]
38. Xiong, J.; Xia, L.; Li, L.; Cui, M.; Gu, Y.; Wang, P. An Acetate-Based NIR Fluorescent Probe for Selectively Imaging of Hydrogen Peroxide in Living Cells and in Vivo. *Sens. Actuators B Chem.* **2019**, *288*, 127–132. [[CrossRef](#)]
39. Yu, X.; Gong, Y.; Xiong, W.; Li, M.; Zhao, J.; Che, Y. Turn-on Fluorescent Detection of Hydrogen Peroxide and Triacetone Triperoxide via Enhancing Interfacial Interactions of a Blended System. *Anal. Chem.* **2019**, *91*, 6967–6970. [[CrossRef](#)]
40. Han, X.; Tian, C.; Yuan, M.S.; Li, Z.; Wang, W.; Li, T.; Chen, S.W.; Wang, J. Colorimetric Hydrazine Detection and Fluorescent Hydrogen Peroxide Imaging by Using a Multifunctional Chemical Probe. *Anal. Chim. Acta* **2019**, *1052*, 137–144. [[CrossRef](#)]
41. Ahmed, S.R.; Cirone, J.; Chen, A. Fluorescent Fe<sub>3</sub>O<sub>4</sub> Quantum Dots for H<sub>2</sub>O<sub>2</sub> Detection. *ACS Appl. Nano Mater.* **2019**, *2*, 2076–2085. [[CrossRef](#)]

42. Ahmed, A.; Hayat, A.; Nawaz, M.H.; John, P.; Nasir, M. Construction of Sponge-like Graphitic Carbon Nitride and Silver Oxide Nanocomposite Probe for Highly Sensitive and Selective Turn-off Fluorometric Detection of Hydrogen Peroxide. *J. Colloid Interface Sci.* **2019**, *558*, 230–241. [[CrossRef](#)] [[PubMed](#)]
43. Wu, Y.; Gao, Y.; Du, J. Bifunctional Gold Nanoclusters Enable Ratiometric Fluorescence Nanosensing of Hydrogen Peroxide and Glucose. *Talanta* **2019**, *197*, 599–604. [[CrossRef](#)] [[PubMed](#)]
44. Sarhan, R.M.; El-Nagar, G.A.; Abouserie, A.; Roth, C. Silver-Iron Hierarchical Microflowers for Highly Efficient H<sub>2</sub>O<sub>2</sub> Nonenzymatic Amperometric Detection. *ACS Sustain. Chem. Eng.* **2019**, *7*, 4335–4342. [[CrossRef](#)]
45. Zhou, J.; Chen, Y.; Lan, L.; Zhang, C.; Pan, M.; Wang, Y.; Han, B.; Wang, Z.; Jiao, J.; Chen, Q. A Novel Catalase Mimicking Nanocomposite of Mn(II)-Poly-L-Histidine-Carboxylated Multi Walled Carbon Nanotubes and the Application to Hydrogen Peroxide Sensing. *Anal. Biochem.* **2019**, *567*, 51–62. [[CrossRef](#)]
46. Riaz, M.A.; Zhai, S.; Wei, L.; Zhou, Z.; Yuan, Z.; Wang, Y.; Huang, Q.; Liao, X.; Chen, Y. Ultralow-Platinum-Loading Nanocarbon Hybrids for Highly Sensitive Hydrogen Peroxide Detection. *Sens. Actuators B Chem.* **2019**, *283*, 304–311. [[CrossRef](#)]
47. Mani, V.; Shanthi, S.; Peng, T.K.; Lin, H.Y.; Ikeda, H.; Hayakawa, Y.; Ponnusamy, S.; Muthamizhchelvan, C.; Huang, S.T. Real-Time Quantification of Hydrogen Peroxide Production in Living Cells Using NiCo<sub>2</sub>S<sub>4</sub>@CoS<sub>2</sub> Heterostructure. *Sens. Actuators B Chem.* **2019**, *287*, 124–130. [[CrossRef](#)]
48. Wang, P.; Cao, L.; Chen, Y.; Wu, Y.; Di, J. Photoelectrochemical Biosensor Based on Co<sub>3</sub>O<sub>4</sub> Nanoenzyme Coupled with PbS Quantum Dots for Hydrogen Peroxide Detection. *ACS Appl. Nano Mater.* **2019**, *2*, 2204–2211. [[CrossRef](#)]



© 2020 by the authors. Licensee MDPI, Basel, Switzerland. This article is an open access article distributed under the terms and conditions of the Creative Commons Attribution (CC BY) license (<http://creativecommons.org/licenses/by/4.0/>).